Available online at www.sciencedirect.com
SCIENCE DIRECT®
Journal of Magnetic Resonance 174 (2005) 34–42
JMR Journal of Magnetic Resonance
www.elsevier.com/locate/jmr

Effect of dielectric properties of solvents on the quality factor for a beyond 900 MHz cryogenic probe model

Takashi Horiuchi[a,b], Masato Takahashi[a,b], Jun Kikuchi[a,b], Shigeyuki Yokoyama[a,c,d], Hideaki Maeda[a,b,*]

[a] *RIKEN Genomic Sciences Center, 1-7-22 Tsurumi, Yokohama 230-0045, Japan*
[b] *Graduate School of Integrated Science, Yokohama City University, Tsurumi-ku, Yokohama 230-0045, Japan*
[c] *Graduate School of Science, The University of Tokyo, Bunkyo-ku, Tokyo 113-0033, Japan*
[d] *RIKEN Harima Institute at SPring-8, 1-1-1 Kohto, Mikazuki-cho, Sayo, Hyogo 679-5148, Japan*

Received 30 November 2004; revised 29 December 2004

Abstract

A previous report by Kelly et al. [J. Am. Chem. Soc. 124 (2002) 12013] indicated that the ionic conductivity of aqueous solution produces a significant contribution to the sensitivity loss in high-resolution NMR equipped with a cryogenically cooled probe. The loss in a sample solution contains two contributions: one from the ionic conductivity and the other from the dielectric loss; the latter is especially important at high frequencies such as above 900 MHz. Here, we investigated the effect of the dielectric conductivity on the quality factor of a 930 MHz cryogenic probe model; in particular, it deals with the ionic aqueous solutions and organic solvents commonly used for NMR in biological research and the chemistry of natural compounds. The sample quality factor, Q_s, at first increases with the real part of the relative dielectric permittivity ε' and then saturates. In the case of polar organic solvents, the transverse electric field on the sample decreases with ε', resulting in an increase of Q_s. In the case of non-polar organic solvents, the dielectric conductivity is so small that the gradient of the increase is steep, resulting in much larger Q_s though the ε' is small. The effect of the transverse electric field is negligible if the ε' becomes large, thus the loss for ionic aqueous solution is mainly governed by a loop current induced in the sample solution. As the induced electromotive force is independent of the ε', the Q_s is saturated at high values of ε'. Based on the Q_s obtained with the cryogenic probe model, the sensitivity for the cryogenic probe is expected to be as follows: the loss in sensitivity by loading water is more than 66%, i.e., the effect of the dielectric conductivity of water is remarkable at high frequencies; polar organic solvent suffers much larger losses, which is due to the enhancement of the effective sample resistance by the effect of ε'; a non-polar organic solvent is nearly free of the sensitivity loss as the dielectric conductivity is negligible; the reverse micelle behaves similarly.

Keywords: High magnetic field; Cryogenic probe; Solvent; Dielectric loss; Sensitivity

1. Introduction

Since the invention of pulse-Fourier transform NMR, the history of NMR has progressed by a series of technical revolutions: the development of high-field NMR magnets and highly sensitive triple inverse probe and multi-dimensional pulse sequences has, over the past two decades, turned solution NMR into the most powerful spectroscopic tool in the fields of chemistry and biology [1–3]. Enhancement of the magnetic field strength improves sensitivity and resolution, in addition to extending the study of biological macromolecules to the 900 kDa supermacro range by TROSY (transverse relaxation time optimized spectroscopy) [4–6]. However,

* Corresponding author. Fax: +81 45 508 7360.
E-mail address: maeda@jota.gsc.riken.go.jp (H. Maeda).

1090-7807/$ - see front matter © 2005 Elsevier Inc. All rights reserved.
doi:10.1016/j.jmr.2005.01.004

its inherently low sensitivity is still the most pressing problem for NMR.

Recently, the use of a new type of cryogenic probe has become widespread. Its RF coil and preamplifier are cooled to a cryogenic temperature, which reduces the thermal noise coming from the RF coil and the noise figure of the preamplifier, resulting in an enhancement of its sensitivity by a factor of 3 to 4 compared with a conventional probe [7–9]. Such a cryogenic probe reduces the data acquisition time and moreover it enables us to use low-concentration samples. It begins to open a new era in the fields of drag-screening [10], in-cell NMR [11–14], metabonomics [8,15], and in vivo NMR [16], to say nothing of improving the structural analysis of biological macromolecules. The signal-to-noise ratio (SNR), i.e., the sensitivity, for a cryogenic probe in the frequency domain is expressed as [17]

$$\mathrm{SNR} \propto \frac{\omega B_{1xy} M_0 \Delta V \sqrt{T_2^*}}{\sqrt{4k(R_c T_c + R_s T_s)F}}, \quad (1)$$

where ω is the Larmor angular frequency, B_{1xy} is the field component in the xy plane generated by unit current of the RF coil, M_0 is the magnetization of the sample, ΔV is the sample volume, T_2^* is the overall transverse relaxation time, k is the Boltzmann constant, R_c is the RF coil resistance, T_c is the RF coil temperature, R_s is the effective sample resistance connected in series to the RF coil corresponding to the energy dissipated in the sample, T_s is the sample temperature, and F is the noise figure of the preamplifier. Here, we assumed the acquisition time nearly equals to the T_2^*. When the RF coil is cooled to a cryogenic temperature, both R_c and T_c are reduced by several fold; the maximum sensitivity is obtained if the sample is a perfect insulator, i.e., R_s is equivalent to zero. On the contrary, if the effective sample resistance R_s is finite, the sensitivity is somewhat reduced by the thermal noise due to R_s. The effective sample resistance R_s contains two contributions: one from the ionic conductivity σ_{ion} and the other from the dielectric conductivity $\omega\varepsilon''\varepsilon_0$, where ε'' is the imaginary part of the relative dielectric permittivity and ε_0 is the dielectric permittivity of vacuum [18]. The sum, $\sigma_{ion} + \omega\varepsilon''\varepsilon_0$, is considered to be an effective conductivity.

The effect of the ionic conductivity, σ_{ion}, on the effective sample resistance, R_s, of a 500 MHz NMR cryogenic probe was studied by Kelly et al. [19]; they demonstrated that in the case of an aqueous salt solution or a buffered aqueous solution, the sensitivity of the 500 MHz cryogenic probe is governed by the ionic conductivity, and presented a selection rule for buffer solutions for protein sample preparation based on the value of the ionic conductivity. However, they ignored the effect of the dielectric conductivity, $\omega\varepsilon''\varepsilon_0$, on the sample solution.

The effect of the dielectric conductivity, $\omega\varepsilon''\varepsilon_0$, on the effective sample resistance, R_s, was originally suggested by Gadian and Robinson [20] from the viewpoint of sample heating by proton decoupling and then it was discussed by Hoult and Lauterbur [21] in connection with the NMR sensitivity of a conventional probe. They treated the problem qualitatively and their studies were limited to aqueous salt solutions; quantitative investigations based on the dielectric properties of ionic aqueous solutions and the NMR organic solvents used for biological research and chemistry of natural compounds have not been reported so far. Furthermore, the effect of the real part of the relative dielectric permittivity, ε', has never been explored, although it affects the transverse electric field strength on the sample and thus changes the sample loss. Both effects are demonstrated here on the quality factor of a 930 MHz cryogenic probe model [22,23] in connection with aqueous salt solutions, buffered aqueous solutions, and polar and non-polar organic solvents.

The topics investigated here are as follows: (i) the effective conductivity for aqueous solutions and polar and non-polar organic solvents and (ii) the dependence of the loaded quality factor [24] on the effective conductivity and the ε' for aqueous solutions and polar and non-polar organic solvents. They are discussed in terms of (a) the effect of ε' on the transverse electric field in the sample and (b) the induced loop current in the sample [20,21]; the relative importance of both phenomena is analyzed based on a computer simulation. The effect of the dielectric conductivity and ionic conductivity on the sensitivity of the cryogenic probe will be discussed [25].

2. Experimental

2.1. Sample preparation

The solvents and buffered solutions listed in Table 1 that are commonly used in the NMR spectroscopy were chosen as the test materials. They are divided into three groups: aqueous solutions, polar organic solvents, and non-polar organic solvents. Good buffer solutions such as Mes and Hepes are not adjusted in pH. A reverse micelle was also prepared for comparison [26,27]. The preparation method for the reverse micelles essentially follows the previously reported protocol; first, 750 mM water was pipetted into a vial containing bis(2-ethylhexyl) sulfosuccinate (AOT) [26,27] and pentane, and second, it was vortexed until the solution became clear. The molar ratio of water per AOT was set to 10.

2.2. Relative dielectric permittivity

The frequency dependence of the relative dielectric permittivity was measured on a test sample in the range 200 MHz to 20 GHz with an Agilent model 85070D dielectric probe kit. The kit has an open-ended coaxial probe, which is immersed in a sample solution. The

Table 1
The ε', effective conductivity $\sigma_{ion} + \omega\varepsilon''\varepsilon_0$, loaded quality factor Q_L, sample quality factor Q_s, sensitivity factor L, and relative sensitivity gain for samples

Sample	ε'	$\sigma_{ion} + \omega\varepsilon''\varepsilon_0$ (S/m)	Q_L	Q_s	Sensitivity factor L	Relative sensitivity gain
Unloaded case	1	0	1480		1.00	7.7
Aqueous solution						
Water	79	0.2	1080	3996	0.34	2.8
100 mM NaCl	78	1.26	460	667	0.15	1.5
50 mM Mes	79	0.24	1015	3231	0.31	2.6
50 mM Hepes	80	0.32	940	2576	0.28	2.4
50 mM K-phosphate (pH 7.0)	79	1.03	540	850	0.17	1.6
50 mM Na-phosphate (pH 4.1)	78	1.41	442	630	0.14	1.5
Polar organic solvent						
DMSO	47	0.24	915	2397	0.27	2.3
Trifluoroethanol	21	0.47	452	651	0.15	1.5
Chloroform–methanol	18	0.30	585	967	0.18	1.7
Methanol	31	0.38	619	1064	0.19	1.7
Ethanol	16	0.52	340	441	0.12	1.4
Propanol	8	0.35	270	330	0.11	1.3
Butanol	5	0.26	300	376	0.11	1.3
Acetone	22	0.03	1377	19786	0.63	5.0
Pyridine	14	0.03	1270	8950	0.48	3.8
Chloroform	6	0.02	1350	15369	0.58	4.6
Non-polar organic solvent						
Hexane	2	0.001	1475	436600	0.97	7.5
Benzene	2	0.001	1480	—	1	7.7
Pentane	2	0.002	1460	108040	0.89	6.9
Reverse micelle	2	0.007	1389	22590	0.66	5.2

end of the cable is connected to an Agilent model E8362B or 8753ES network analyzer, which gives the frequency dependence of the following parameter [28]:

$$\varepsilon' - \mathrm{i}\left(\frac{\sigma_{ion}}{\omega\varepsilon_0} + \varepsilon''\right). \quad (2)$$

The effective conductivity, $\sigma_{ion} + \omega\varepsilon''\varepsilon_0$, is derived from the imaginary part of the parameter.

2.3. Quality factor for a 930 MHz NMR probe model

A 930 MHz NMR cryogenic probe model, as seen in Fig. 1, was developed to measure the loaded quality factor, denoted as Q_L. The probe model consists of a vacuum vessel evacuated to less than 10^{-6} mmHg that was 320 mm in diameter and 240 mm in height, an RF coil, a cold head for cooling the RF coil, a semi-rigid signal cable, and a set of tuning and matching condensers. An Alderman and Grant type of RF coil [29] was contacted to the cold head, indirectly cooled by liquid helium flow from a container. The tuning and matching condensers were soldered to the RF coil, and were adjustable from the bottom.

The Alderman and Grant type of RF coil, 10.7 mm in inner diameter and 57 mm in length, was formed around an outer glass tube. A 5 mm wide shield ring was bonded on the inner surface of the glass tube near the bottom of the RF coil. Another inner glass tube ensures a vacuum-seal by an O-ring against the vacuum vessel. A pair of

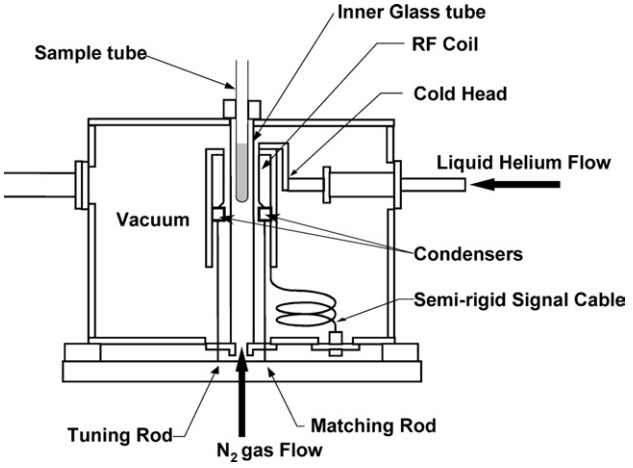

Fig. 1. A cross-sectional view of the cryogenic probe model. The RF coil is cooled to 15 K and then an NMR sample tube is loaded in the bore. After the RF circuit is tuned to 930 MHz and matched, the loaded quality factor Q_L is measured by a network analyzer.

20 mm wide shield rings is bonded to the inner glass tube. Room temperature nitrogen gas flows through the inner glass tube during the experiment, which keeps the sample temperature at 300 K.

First, the RF coil is cooled to 15 K and then an NMR sample tube is loaded in the bore of the probe model. After the RF circuit is tuned to 930 MHz and matched to 50 Ω, the Q_L was measured by an Agilent model 8753ES network analyzer.

3. Experimental results

3.1. Dielectric characteristics and effective conductivity

The frequency dependence of ε' and $\sigma_{ion}/(\omega\varepsilon_0) + \varepsilon''$ for water, 100 mM NaCl solution, methanol, pyridine, and pentane is shown in Fig. 2; the frequency dependence of effective conductivity, $\sigma_{ion} + \omega\varepsilon''\varepsilon_0$, is shown in Fig. 3. For water, ε' and ε'' are described by the Debye function; the ε' at high frequencies, ε_∞, and at low frequencies, $\varepsilon(0)$, are 79.5 and 5.0, respectively, while the dielectric relaxation time, τ, is 9.2×10^{-12} s. The relaxation time corresponds to the time that water molecules dwell in their ground state of water clusters, before being activated to the mobile state [28]. The results coincide with those reported previously [30–34].

The effective conductivity for water is governed by the dielectric conductivity and it is as high as 0.20 S/m at 930 MHz, which is equivalent to the ionic conductivity for a 20 mM NaCl solution. For 100 mM NaCl solution, the effective conductivity is 1.26 S/m at 930 MHz;

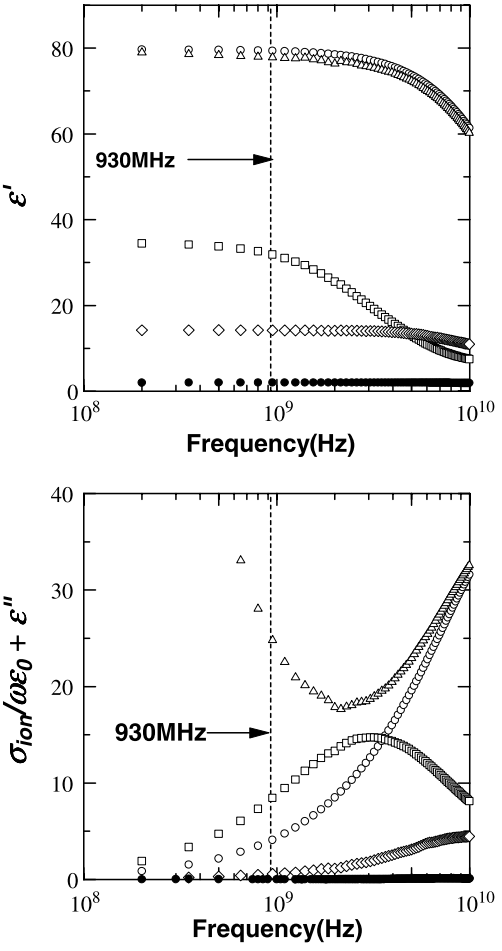

Fig. 2. The frequency dependence of ε' and $\sigma_{ion}/(\omega\varepsilon_0) + \varepsilon''$ for water (○), 100 mM NaCl (△) aqueous solution, methanol (□), pyridine (◇), and pentane (●).

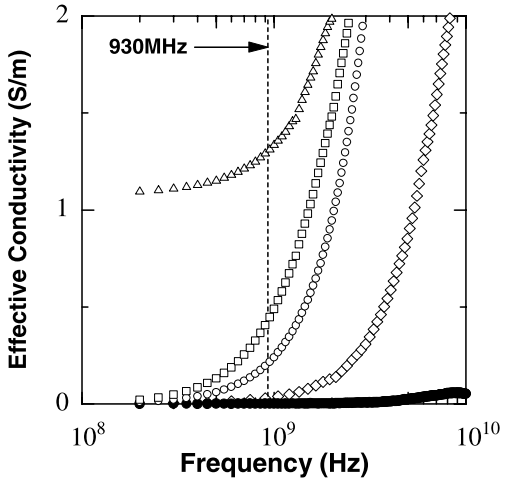

Fig. 3. The effective conductivity $\sigma_{ion} + \omega\varepsilon''\varepsilon_0$ for typical sample solutions: water (○); 100 mM NaCl (△); methanol (□); pyridine (◇); pentane (●).

it is governed by the ionic conductivity of NaCl at low frequencies, while both the ionic conductivity of NaCl and the dielectric conductivity of water contribute similar effects above 2 GHz. The effect of the ionic conductivity was also important for phosphate buffers. For good buffers, such as Hepes and Mes, the effective conductivity is dominated by the dielectric conductivity of buffer molecules and water at low frequencies, while it is governed by the dielectric conductivity of water above 2 GHz.

For the polar organic solvent, methanol, ε'' shows a peak at 3.1 GHz and the effective conductivity is dominated by the dielectric conductivity; it is 0.38 S/m at 930 MHz as seen in Fig. 3. The effective conductivities for other alcohols are in the range 0.26–0.52 S/m at 930 MHz, while their ε' values lie in the range 5–31. Though acetone, pyridine, and chloroform belong to the polar organic solvent group, their effective conductivities are less than 1/10 of the alcohols (i.e., 0.02–0.03 S/m), while their ε' values are similar to alcohols (see Figs. 2 and 3). For the non-polar organic solvent, pentane, Fig. 3 shows that the effective conductivity is as small as 0.002 S/m at 930 MHz and its ε' is as small as 2.0. The effective conductivity for the reverse micelle is threefold larger than that for pentane, while the micelle's ε' is the same as that of pentane. The ε' and effective conductivity for aqueous solutions, and polar and non-polar organic solvents are listed in Table 1.

3.2. Loaded quality factor, Q_L

The unloaded quality factor, denoted as Q_0, is defined here as the quality factor when the probe is loaded with an empty NMR sample tube. The sample quality factor, denoted as Q_s, is defined to be the quality factor that will result if an RF coil is loss free and only a sample loss is

loaded [35]. Then, the loaded quality factor, Q_L, is expressed as

$$\frac{1}{Q_L} = \frac{1}{Q_0} + \frac{1}{Q_s}. \quad (3)$$

Here, the Q_s is given by

$$Q_s = \frac{\omega L}{R_s}, \quad (4)$$

where L is the RF coil inductance. Note that the Q_s is inversely proportional to the effective sample resistance, R_s.

The Q_L for aqueous solutions listed in Table 1 is shown by the closed circles (●) in Fig. 4. TheQ_0 is 1480 as given by the open circle (○). The Q_L monotonically decreases with the effective conductivity of the aqueous solution; e.g. the Q_L for water is 1080, and that for 100 mM NaCl solution is 460. The effective conductivity of 5 S/m in Fig. 4 corresponds to a 500 mM NaCl solution ($Q_L = 170$). The $1/Q_s$ value was proportional to the effective conductivity as we assumed in this paper; the broken line in Fig. 4 indicates this proportionality. More details will be discussed later based on the equivalent-circuit model.

For polar organic solvents such as alcohols, the Q_L is notably degraded relative to aqueous solutions as seen by the open squares (□) in Fig. 4, although their effective conductivities are close to the value for water. Thus, it is clear that the sample loss for a polar organic solvent is governed by a different process from the case of water. The Q_s for polar organic solvents are plotted as the closed circles (●) against ε' in Fig. 5; the Q_s for water

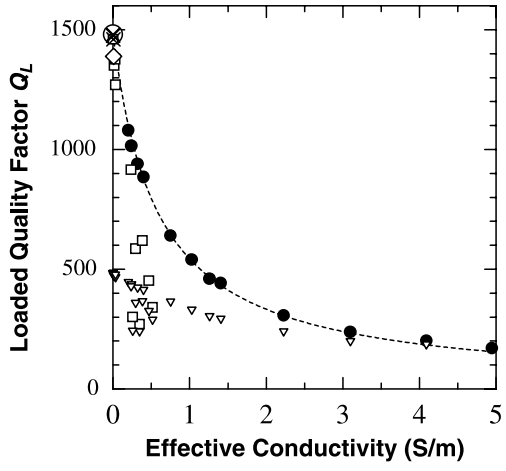

Fig. 4. Effective conductivity dependence of the loaded quality factor Q_L for the 930 MHz cryogenic probe model at 15 K for aqueous solutions (●), polar organic solvents (□), and non-polar organic solvents (×). The Q_L for a reverse micelle (◇) is also shown for comparison. The unloaded quality factor Q_0 is given by the open circle (○). The broken line shows the proportionality of $1/Q_s$ against the effective conductivity. The Q_L measured by a room temperature probe is also shown for comparison (▽).

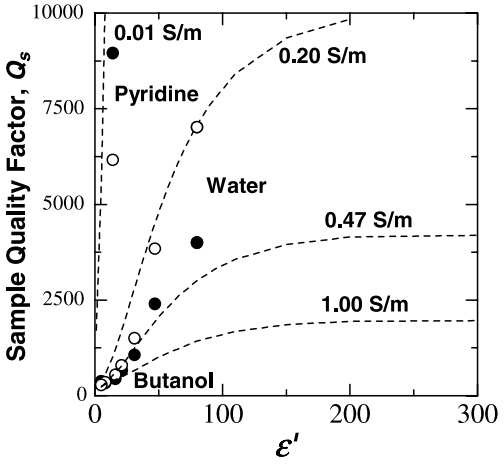

Fig. 5. Sample quality factor dependence on the ε' for polar organic solvents and water: The Q_s increases with ε' at first and then saturates, as shown by the simulation curve (the broken line). The experimental results (●) agree with the simulation results (○).

is also included for comparison. For polar organic solvents, such as DMSO, trifluoroethanol, chloroform–methanol, methanol, ethanol, propanol and butanol, and water, Q_s increases with the ε' at first and then tends to saturate. On the contrary, for polar organic solvents with smaller effective conductivities, such as pyridine, acetone, and chloroform, the values of Q_s are as large as 10^4 for pyridine, which is 10-fold larger than those for the alcohols shown in Fig. 5. Thus, the Q_L is close to the Q_0, which is in the range 1270–1377. Similarly, for non-polar organic solvents, such as hexane, benzene and pentane, Table 1 shows that the Q_s values are larger than 10^5, and thus the Q_L nearly coincides with the Q_0, although the ε' is small, $\varepsilon' = 2$. The Q_L for the reverse micelle is 1389, which is only 5% smaller than that for pentane; the effect of the micelle and the water inside on the Q_L is nearly negligible. Thus, it is shown that both the ε' and the effective conductivity of the sample solution affect the Q_s for organic solvents.

4. Simulations

The schematics of the RF coil and the surrounding parts were imported to the electromagnetic simulation software "CST Microwave Studio ver. 4" that is based on the finite integration technique [36]. The mesh model of the sample and RF coil is generated automatically by a mesh generator taking into account specific electromagnetic characteristics of the structure. The electromagnetic simulation is performed in the time domain, stimulating Gaussian-shaped pulses with a broad-band frequency spectrum that includes 930 MHz. During the simulation, a discrete Fourier transformation is performed for the transient field component on all mesh nodes. Then, electromagnetic field amplitude and phase

components specifically at a 930 MHz frequency were extracted over the calculation domain. Both vector and scalar data field components could be plotted in the contour and arrow plot representations. The boundary region of the simulation domain is taken as a perfect electric conductivity wall to contain the RF power, an assumption that meets well the actual experimental condition. The conduction current density in the sample is evaluated by the internal electric field strength and electroconductivity of the material. The sample quality factor, Q_s, is estimated by the ratio between the product of ω and the time-averaged total energy stored in the whole structure to the energy loss per second in the sample.

The ε' dependence of the simulated Q_s is shown by the broken line in Fig. 5, the nature of which is summarized as follows:

1. The Q_s increases with the increase of ε' at first and then saturates. The gradient increases with a decrease of the effective conductivity.
2. The saturation Q_s is inversely proportional to the effective conductivity.

Both the conduction current density and the electric field are calculated in the midplane perpendicular to the RF magnetic field (see Figs. 6A and B); they are shown in Fig. 6C for butanol, which has one of the smallest Q_s in Fig. 5. The conduction current density, indicated by the arrow, oscillates back and forth in the transverse direction between both legs of the RF coil at 930 MHz. The electric field strength in the sample, indicated by the contour, is in the range 360–1400 V/m.

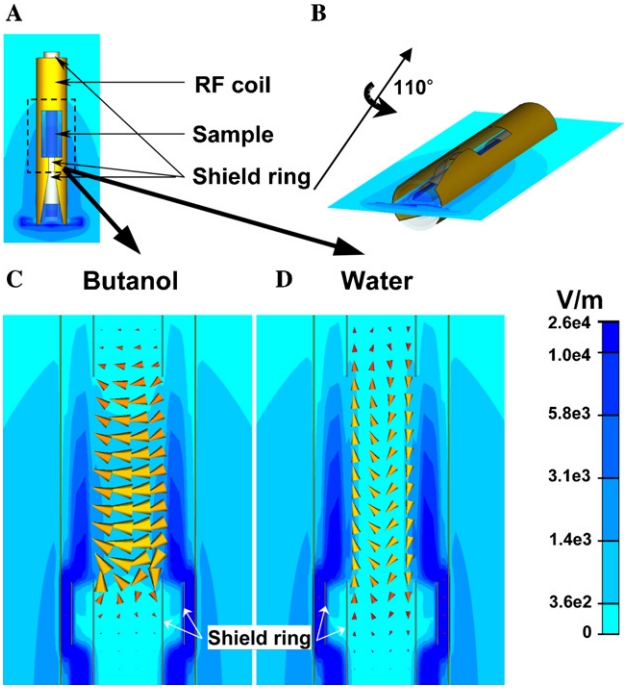

Fig. 6. (A) The simulation model of the electromagnetic field. (B) The viewing angle of the model in (A) has been changed to show the plane through the middle of the RF coil in blue. (C) The current distribution and the electric field distribution in the midplane, perpendicular to the RF magnetic field for butanol. The transverse current oscillates at 930 MHz. (D) The current distribution and the electric field distribution for water. The loop current is induced in the sample solution.

The experimental Q_s values (●) for DMSO, methanol, trifluoroethanol, ethanol, propanol, butanol, and pyridine agree with the simulation Q_s values (○) as shown in Fig. 5. The gradient for pyridine is 10-fold steeper than that of a typical alcohol, as the effective conductivity is 1/10 of that of the alcohols; thus, the experimental Q_s for pyridine becomes large, 8950, even though its ε' is as small as 14. Similarly, the gradient for non-polar organic solvents is 100-fold steeper than that of alcohol and therefore the Q_s becomes 10^5, even though the ε' assumes a negligible value such as 2. Thus, it is demonstrated that the Q_s for polar and non-polar organic solvent is governed by the effective conductivity caused by the transverse electric field on the sample.

The ε' dependence of the sample quality factor Q_s is qualitatively explained by the equivalent-circuit model for representing the sample loss by the transverse voltage as seen in Fig. 7: the transverse voltage V between RF coil legs is divided by an air gap capacitor C_g and a sample capacitor $\varepsilon' C_s$, connected in series; here, $1/(\omega\varepsilon'' C_s)$ represents the sample dielectric loss. According to Minard and Wind [37], the effective sample resistance, R_s, for the circuit element is described as

$$R_s = \frac{C_g^2}{(\varepsilon'' C_s)^2 + (C_g + \varepsilon' C_s)^2}(\omega L)^2(\omega\varepsilon'' C_s). \tag{5}$$

If we assume $\varepsilon' \gg \varepsilon''$ as seen in Fig. 2, we obtain the simple expression,

$$R_s = \left[\frac{C_g}{(C_g + \varepsilon' C_s)}\omega L\right]^2(\omega\varepsilon'' C_s). \tag{6}$$

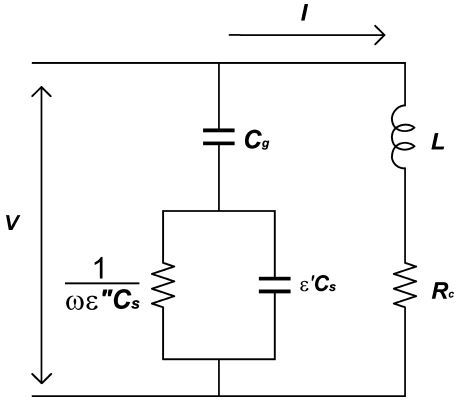

Fig. 7. The equivalent-circuit model for representing the dielectric sample loss caused by the transverse voltage: C_g is the gap capacitor, $\varepsilon' C_s$ is the sample capacitor, $1/\omega\varepsilon'' C_s$ is the dielectric loss, L is the RF coil inductance, R_c is the RF coil resistance, V is the transverse voltage, and I is the RF coil current.

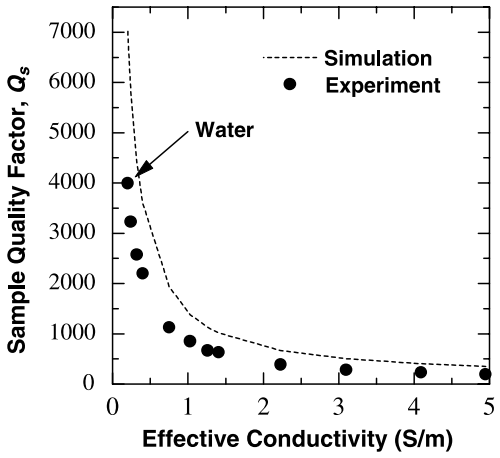

Fig. 8. Sample quality factor dependence on the effective conductivity for aqueous solutions. The experimental results (●) agree with the simulation results indicated by the broken line.

The first bracket is proportional to the transverse sample voltage, which decreases with the increase of ε'. We then have

$$Q_s = \left(\frac{C_g + \varepsilon' C_s}{C_g}\right)^2 \left(\frac{1}{\omega L}\right)\left(\frac{1}{\omega \varepsilon'' C_s}\right). \tag{7}$$

Thus, theQ_s increases with an increase in ε' and it is inversely proportional to the effective conductivity.

Fig. 6D shows the conduction current density and the electric field for water, which is near the saturation line seen in Fig. 5. The transverse sample voltage decreases with ε', and if the voltage becomes less than the circumferential electromotive force (EMF) induced by the mutual inductance between the RF coil and a sample solution, the EMF dominates the current in the sample [38]. Thus, the transverse current density seen in Fig. 6C nearly disappears as the ε' for water is as large as 79. Moreover, the electric field strength in the sample is less than 360 V/m: the EMF induces a current loop oscillating in the clockwise and anticlockwise direction at 930 MHz. As the EMF is independent of the value of ε', the Q_s saturates with ε' for $\varepsilon' > 100$, as seen in Fig. 5. The simulated Q_s values for aqueous solutions listed in Table 1 agreed with the experimental Q_s values with a deviation of 40% (see Fig. 8). Thus, it is clear that the Q_s for aqueous solution is mainly governed by the induced loop current in the sample; note that only the dielectric conductivity contributes to the loop current in case of water, while both the ionic conductivity and the dielectric conductivity contribute in the case of ionic aqueous solutions.

5. Discussion

The sensitivity factor introduced by Kelly et al. [19] is used here as the ratio of the sensitivity for a loaded cryogenic probe, denoted as $\mathrm{SNR_L}$, to the sensitivity for a cryogenic probe loaded by a loss-free solvent, denoted as $\mathrm{SNR_0}$; the latter corresponds to the maximum achievable sensitivity for a probe. Then, the sensitivity factor L is given as

$$\begin{aligned} L &= \frac{\mathrm{SNR_L}}{\mathrm{SNR_0}} \\ &= \left(\frac{\omega B_{1xy} M_0 \Delta V \sqrt{T_2^*}}{\sqrt{4k(T_c R_c + T_s R_s)F}}\right) \Big/ \frac{\omega B_{1xy} M_0 \Delta V \sqrt{T_2^*}}{\sqrt{4kT_c R_c F}} \\ &= \sqrt{\frac{15R_c}{15R_c + 300R_s}} = \sqrt{\frac{1}{1 + 20Q_0/Q_s}}, \end{aligned} \tag{8}$$

where $T_c = 15$ K and $T_s = 300$ K are used; note that the sensitivity factor assumes the same height of the spectral peak for all solvents. Based on the experimental Q_0 and Q_s values, the sensitivity factor shown in Table 1 was obtained. The sensitivity factor for water is 0.34, much lower than that, i.e., 0.98, reported for a 500 MHz NMR cryogenic probe [19]. Considering the proportionality to ω^3 seen in Eq. (6) and the frequency dependence of the ε'', the R_s for water at 930 MHz is 10-fold larger than that at 500 MHz, which results in greater loss of sensitivity for water at 930 MHz. The sensitivity factor for aqueous solutions decreases with the effective conductivity of the solution to reach 0.15 at 1.26 S/m, corresponding to a 100 mM NaCl solution, and then gradually approaches to zero. Thus, it is clear that as far as aqueous solutions are concerned, the sensitivity factor is limited to be less than 34% of the maximum achievable sensitivity at 930 MHz, due to the dielectric conductivity of water.

The sensitivity factor for organic solvents such as DMSO, trifluoroethanol, chloroform–methanol, methanol, ethanol, propanol, and butanol is in the range 0.11–0.27; most of them have a much worse value than water, due to the enhanced effective sample resistance seen in Eq. (6). For chloroform, pyridine, and acetone, the sensitivity factor is in the range 0.48–0.63, better than that for water. For non-polar organic solvents such as hexane, benzene, and pentane, the sensitivity factor is in the range 0.89–1.0; they will nearly achieve the $\mathrm{SNR_0}$.

The Q_L at room temperature was measured and is plotted by an empty down triangle (▽) in Fig. 4. The ratio of the sensitivity for an unloaded room temperature probe, $\mathrm{SNR_{0,300\,K}}$, to that for an unloaded cryogenic probe, $\mathrm{SNR_{0,15\,K}}$, is given by

$$\frac{\mathrm{SNR_{0,300\,K}}}{\mathrm{SNR_{0,15\,K}}} = \frac{\sqrt{15R_{c,15\,K}}}{\sqrt{300R_{c,300\,K}}} = \sqrt{\frac{Q_{0,300\,K}}{20Q_{0,15\,K}}} = 0.13, \tag{9}$$

where $R_{c,300\,K}$ and $R_{c,15\,K}$ are the RF coil resistances at room temperature and at 15 K, respectively, and $Q_{0,300\,K}$ and $Q_{0,15\,K}$ are the unloaded quality factor values in Fig. 4 at room temperature and at 15 K, respec-

tively. The ratio of $L_{15\,K}/(0.13L_{300\,K})$ gives the relative sensitivity gain by the cryogenic probe, where the $L_{15\,K}$ and $L_{300\,K}$ are the sensitivity factor at 15 K and at room temperature, respectively; they are 2.8 for water; 1.5 for 100 mM NaCl solution; 1.3 for butanol; 1.7 for methanol; 4.6 for chloroform; and 6.9 for pentane (see Table 1). It is clear that the sensitivity gain for a cryogenic probe loaded by an aqueous solution is less than 2.8, limited by the dielectric loss of water. On the contrary, in the case of non-polar organic solvents, the effective sample resistance is insignificant and the cryogenic probe achieves the maximum attainable sensitivity gain. Thus, from the viewpoint of sample noise, non-polar organic solvents are expected to be the best choice for a very high-field NMR spectrometer. Furthermore, it is probable that if the RF coil temperature is decreased from 15 to 4 K, the sensitivity gain may be double of that at 15 K, assuming the sample loss for a non-polar organic solvent is negligible [23]. The use of non-polar organic solvents is common in the field of chemical analysis of natural compounds or metabolomics studies [39], though low sensitivity is an essential problem in both cases. Our prediction of significant sensitivity gain in non-polar solvents at very high fields will promote the usefulness of cryogenic probe in these areas, although more experiments need to be conducted in this connection. Furthermore, considering the large sensitivity gain of pentane, 6.9, a reverse micelle approach [24] is attractive to overcome the sensitivity loss for aqueous solutions at high fields; in fact, based on these experimental results, the sensitivity gain for a reverse micelle sample is 5.2, much better than that for aqueous solutions.

6. Conclusions

(1) The effective sample resistance contains two contributions: one from the ionic conductivity and the other from the dielectric conductivity. The dielectric conductivity contributes a considerable effect at high frequencies above 900 MHz.

(2) The sample quality factor of the 930 MHz cryogenic probe model increases with the ε' of the sample at first and then saturates. According to the computer simulation, the transverse electric field within the sample decreases with an increase in ε', resulting in an increase in the sample quality factor. The effect of the transverse electric field is negligible if ε' becomes large, and the loss is governed by a loop current induced in the sample.

(3) The loaded quality factor for polar organic solvents and non-polar organic solvents at 930 MHz are governed by the dielectric conductivity due to the transverse electric field, while those for aqueous solutions are governed by the ionic and dielectric conductivity due to the current loop.

(4) An estimate has been made of the sensitivity factor of the loaded cryogenic probe; the sensitivity for aqueous solution sample is less than 34% of the maximum achievable sensitivity of the cryogenic probe due to the dielectric conductivity by water. Polar organic solvent suffers much larger losses, which is due to the enhancement of the effective sample resistance by the effect of ε'. The sensitivity gain for non-polar organic solvent nearly achieves the maximum attainable sensitivity. The large gain for pentane is not degraded by forming a reverse micelle.

Acknowledgments

This work was partly supported by the National Project on Protein Structural and Functional Analysis, Ministry of Education, Culture, Sports, Science and Technology, in Japan, and also supported by the RIKEN Structural Genomics/Proteomics Initiative (RSGI).

References

[1] R.R. Ernst, Nuclear magnetic resonance Fourier transform spectroscopy (Nobel Lecture), Angew. Chem. Int. Ed. Engl. 31 (1992) 805–823.
[2] G.M. Clore, A.M. Gronenborn, Structures of larger proteins in solution: Three-, and four-dimensional heteronuclear NMR spectroscopy, Science 252 (1991) 1390–1399.
[3] A. Bax, S. Grzesiek, Methodological advances in protein NMR, Acc. Chem. Res. 26 (1993) 131–138.
[4] K. Pervushin, R. Riek, G. Wider, K. Wüthrich, Attenuated T_2 relaxation by mutual cancellation of dipole–dipole coupling and chemical shift anisotropy indicates an avenue to NMR structures of very large biological macromolecules in solution, Proc. Natl. Acad. Sci. USA 94 (1997) 12366–12371.
[5] M. Saltzmann, K. Pervushin, G. Wider, H. Senn, K. Wüthrich, TROSY in triple-resonance experiments: New perspectives for sequential NMR assignment of large proteins, Proc. Natl. Acad. Sci. USA 95 (1998) 13585–13590.
[6] J. Flaux, E.B. Bertelsen, A.L. Horwich, K. Wüthrich, NMR analysis of a 900 K GroEL–GroES complex, Nature 418 (2002) 207–211.
[7] R.C. Crouch, W. Llanos, K.G. Mehr, C.E. Hadden, D.J. Russel, G.E. Martin, Applications of cryogenic NMR probe technology to long-range ^{1}H–^{15}N 2D NMR studies at natural abundance, Magn. Reson. Chem. 39 (2001) 555–558.
[8] H.C. Keun, O. Beckonert, L. Griffin, C. Richter, D. Moskau, J.C. Lindon, J.K. Nicholson, Cryogenic probe ^{13}C NMR spectroscopy of urine for metabonomic studies, Anal. Chem. 74 (2002) 4588–4593.
[9] M. Spraul, A.S. Freund, R.E. Nast, R.S. Withers, W.E. Maar, O. Corcoran, Advancing NMR sensitivity for LC-NMR-MS using a cryoflow probe: application to the analysis of acetaminophen metabolites in urine, Anal. Chem. 75 (2003) 1546–1551.
[10] P. Hajduk, T. Gerfin, J.-M. Boehlen, M. Häberli, D. Marek, S.W. Fesik, High-throughput nuclear magnetic resonance-based screening, J. Med. Chem. 42 (1999) 2315–2317.
[11] Z. Serber, A.T. Keatinge-Clay, R. Ledwidge, A.E. Kelly, S. Miller, V. Dötsch, High-resolution macromolecular NMR spec-

troscopy inside living cells, J. Am. Chem. Soc. 123 (2001) 2446–2447.
[12] Z. Serber, R. Ledwidge, S.M. Miller, V. Dötsch, Evaluation of parameters critical to observing proteins inside living *Escherichia coli* by in-cell NMR spectroscopy, J. Am. Chem. Soc. 123 (2001) 8895–8901.
[13] Z. Serber, V. Dötsch, In-cell NMR spectroscopy, Biochemistry 40 (2001) 14317–14323.
[14] Z. Serber, W. Straub, L. Corsini, A.M. Nomura, N. Shimba, C.S. Craik, P.O. de Montellano, V. Dötsch, Methyl groups as probes for proteins and complexes in in-cell NMR experiments, J. Am. Chem. Soc. 126 (2004) 7119–7125.
[15] J.L. Griffin, H. Keun, C. Richter, D. Moskau, C. Rae, J.K. Nicholson, Compartmentation of metabolism probed by [2-^{13}C]alanine: improved ^{13}C NMR sensitivity using a CryoProbe detects evidence of a glial metabolon, Neurochem. Int. 42 (2003) 93–99.
[16] C. Hinse, C. Richter, A. Provenzani, J. Stöckigt, In vivo monitoring of alkaloid metabolism in hybrid plant cell cultures by 2D cryo-NMR without labelling, Bioorg. Med. Chem. 11 (2003) 3913–3919.
[17] D.I. Hoult, Encyclopedia of Nuclear Magnetic Resonance, vol. 7, Wiley, New York, 1996, pp. 4256–4266.
[18] D.M. Pozer, Microwave Engineering, Wiley, New York, 1998.
[19] A.E. Kelly, H.D. Ou, R. Withers, V. Dötsch, Low-conductivity buffers for high-sensitivity NMR measurements, J. Am. Chem. Soc. 124 (2002) 12013–12019.
[20] D.G. Gadian, F.N.H. Robinson, Radiofrequency losses in NMR experiments on electrically conducting sample, J. Magn. Reson. 34 (1979) 449–455.
[21] D.I. Hoult, P.C. Lauterbur, The sensitivity of the zeugmatographic experiment involving human samples, J. Magn. Reson. 34 (1979) 425–433.
[22] T. Kiyoshi, H. Maeda, J. Kikuchi, Y. Ito, H. Hirota, S. Yokoyama, S. Ito, T. Miki, M. Hamada, O. Ozaki, S. Hayashi, N. Kurihara, H. Suematsu, M. Yoshikawa, S. Matsumoto, A. Sato, H. Wada, Present status of 920 MHz high-resolution NMR spectrometers, IEEE Trans. Appl. Superconduct. 14 (2004) 1608–1612.
[23] H. Yokota, T. Okamura, Y. Ohtani, T. Kuriyama, M. Takahashi, J. Kikuchi, S. Yokoyama, H. Maeda, 4.5 K cooling system for a cryogenically cooled probe for 920 MHz NMR, Adv. Cryog. Eng. 49 (2004) 1826–1833.
[24] P.F. Flynn, D.L. Mttiello, H.D. Hill, A.J. Wand, Optimal use of cryogenic probe technology in NMR studies of proteins, J. Am. Chem. Soc. 122 (2000) 4823–4824.
[25] T. Horiuch, M. Takahashi, J. Kikuchi, H. Yokota, S. Yokoyama, H. Maeda, Effect of solvents on the quality factor for a 930 MHz cryogenic probe model, in: 45th ENC, Asilomar, CA, 2004, long abstract E040314.pdf.
[26] C.R. Babu, P.F. Flynn, A.J. Wand, Validation of protein structure from preparations of encapsulated proteins dissolved in low viscosity fluids, J. Am. Chem. Soc. 123 (2001) 2691–2692.
[27] C.R. Babu, P.F. Flynn, A.J. Wand, Preparation, characterization, and NMR spectroscopy of encapsulated proteins dissolved in low viscosity fluids, J. Biomol. NMR 25 (2003) 313–323.
[28] R. Buchner, G.T. Hefter, P.M. May, Dielectric relaxation of aqueous NaCl solutions, J. Phys. Chem. 103 (1999) 1–9.
[29] D.W. Alderman, D.M. Grant, An efficient decoupler coil design which reduces heating in conductive samples in superconducting spectrometers, J. Magn. Reson. 36 (1979) 447–451.
[30] J. Barthel, R. Buchner, M. Munsterer, Electrolyte Data Collection Part 2: Dielectric Properties of Water and Aqueous Electrolyte Solutions, DECHEMA, Federal Republic of Germany, 1995.
[31] I. Bunget, M. Propescu, Physics of Solid Dielectrics, Elsevier, New York, 1984.
[32] N.E. Dorsey, Properties of Ordinary Water–Substance, Reinhold Publishing, New York, 1940.
[33] U. Kaatze, V. Uhlendorf, The dielectric properties of water at microwave frequencies, Z. Phys. Chem. 126 (1981) 151–165.
[34] S. Gabriel, R.W. Lau, C. Gabriel, The dielectric properties of biological tissues: III. Parametric models for the dielectric spectrum of tissues, Phys. Med. Biol. 41 (1996) 2271–2293.
[35] R.E. Collin, Foundations for Microwave Engineering, Wiley, New York, 2001.
[36] T. Weiland, A discretization method for the solution of Maxwell's equations for six-component fields, Electron. Commun. 31 (1977) 116–120.
[37] M.R. Minard, R.A. Wind, Solenoidal microcoil design—Part II: Optimizing winding parameters for maximum signal-to-noise performance, Concepts Magn. Reson. 13 (2001) 190–210.
[38] C.N. Chen, D.I. Hoult, Biomedical Magnetic Resonance Technology, Institute of Physics Publishing, Bristol, 1989.
[39] J. Kikuchi, K. Shinozaki, T. Hirayama, Stable isotope labeling of *Arabidopsis thaliana* for an NMR-based metabolomics approach, Plant Cell Physiol. 45 (2004) 1099–1104.